

Dual band sensitivity enhancements of a VO_x microbolometer array using a patterned gold black absorber

EVAN M. SMITH,^{1,2,*} DEEP PANJWANI,¹ JAMES GINN,² ANDREW P. WARREN,¹ CHRISTOPHER LONG,² PEDRO FIGUIEREDO,^{1,2} CHRISTIAN SMITH,¹ JANARDAN NATH,¹ JOSHUA PERLSTEIN,² NICK WALTER,³ CAROL HIRSCHMUGL,³ ROBERT E. PEALE,¹ AND DAVID SHELTON²

¹Department of Physics, University of Central Florida, Orlando, Florida 32816, USA

²Plasmonics, Inc., 12605 Challenger Pkwy STE 150, Orlando, Florida 32826, USA

³Department of Physics, University of Wisconsin-Milwaukee, Milwaukee, Wisconsin 53211, USA

*Corresponding author: evansmith@knights.ucf.edu

Received 12 October 2015; revised 31 December 2015; accepted 28 January 2016; posted 1 February 2016 (Doc. ID 251710); published 10 March 2016

Infrared-absorbing gold black has been selectively patterned onto the active surfaces of a vanadium-oxide-based infrared bolometer array. Patterning by metal lift-off relies on protection of the fragile gold black with an evaporated oxide, which preserves much of gold black's high absorptance. This patterned gold black also survives the dry-etch removal of the sacrificial polyimide used to fabricate the air-bridge bolometers. For our fabricated devices, infrared responsivity is improved 22% in the long-wave IR and 70% in the mid-wave IR by the gold black coating, with no significant change in detector noise, using a 300°C blackbody and 80 Hz chopping rate. The increase in the time constant caused by the additional mass of gold black is ~15%. © 2016 Optical Society of America

OCIS codes: (040.3060) Infrared; (040.6808) Thermal (uncooled) IR detectors, arrays and imaging; (310.3915) Metallic, opaque, and absorbing coatings.

<http://dx.doi.org/10.1364/AO.55.002071>

1. INTRODUCTION

Heating by absorbed infrared power causes a measurable change in bolometer resistance. Increasing absorption with an optical or plasmonic resonant coating can increase responsivity without increasing noise, in principle. Optimization for mid-wave IR (MWIR, 3–5 μm wavelength) or long-wave IR (LWIR, 8–12 μm wavelength) is usually achieved by Fabry–Perot [1,2] or other resonant structures [3–5], whose peak absorption and bandwidth depend on resonator *Q* and hence on fabrication tolerances. Typically, high absorptance can be achieved using these methods, but the bandwidth is often limited. Chang [6] developed a dual cavity structure using a spacer layer to increase the bandwidth of the absorption for LWIR, but the average absorption was only 59% and 65% for 8–9.4 μm and 9.4–10.8 μm, respectively. Alternatively, Aggoun [7] modeled a cavity structure in which the peak absorption at 9.8 μm was 96% with an average absorption over 90% for LWIR. Using tight control of fabrication processes and a silicon nitride stack, Raytheon is able to produce focal plane arrays with absorption exceeding 80% [8] averaged over the LWIR. The combination of Fabry–Perot resonant structure

and gold black coating that we report here achieves a nearly flat 90% absorptance across both LWIR and MWIR bands and hence evidently exceeds the state of the art. Microbolometers may never compete with photon-sensitive devices in the MWIR in terms of sensitivity [9], but simultaneous high response in *both* MWIR and LWIR may have certain desirable applications. While the LWIR is the most useful range for room-temperature scenes, MWIR capability is necessary to detect rocket plumes, directional infrared counter measures lasers, seeing in haze or marine aerosol, or achieving high dynamic range that is not supported by a single band [10].

Gold black has very high absorption over a broad spectral range [11]. Blanket coatings are easily achieved using an ordinary thermal evaporator, suggesting the possibility of multi-band sensors fabricated using a single material with minimal fabrication tolerances. On the other hand, this low-density material is extremely fragile, which makes it difficult to integrate onto a microbolometer array, since usual fabrication processes destroy the film. Some of us recently demonstrated patterning of gold black by usual lift-off enabled by an evaporated SiO₂ protection layer [12,13]. Such protected gold black

retains high absorption in the MWIR and LWIR bands [12]. Meanwhile, Plasmonics, Inc. has developed high-performance room-temperature air-bridge microbolometer arrays using amorphous vanadium oxide (VO_x) thin films [14,15]. These detectors achieve a projected absorptance of 71%, as determined by numerical calculation, in the LWIR but are not designed to function well in the MWIR.

Our preliminary report of bolometer responsivity enhancement due to patterned gold black was presented in [16]. Here, we present new results and analysis, particularly in the MWIR and LWIR bands, using an optimized detector design. Revised analysis of the thermal response time of the microbolometer indicates that the addition of gold black marginally decreases the speed of the detector, but response is enhanced and more uniform in both MWIR and LWIR bandwidths. These observed increases would indeed be smaller for more optimized devices, such as those fabricated by Raytheon [8]. However, this demonstration shows the possibility of achieving high absorption in cases where a cavity is not possible or high tolerance of structure dimensions is not easily achieved. While D^* of our fabricated devices only reaches $10^7 \text{ cm Hz}^{1/2} \text{ W}^{-1}$, we conclude that this is due to high $1/f$ noise and is unrelated to the application of the gold black absorber. Finally, the effects of thermal treatments characteristic of the usual packaging processes are discussed.

2. THEORETICAL CONSIDERATIONS

Figure 1 presents a schematic diagram for the air-bridge microbolometer developed for testing. The structure is built upon an oxidized substrate for electrical isolation. Nichrome (80/20 nickel–chromium) is chosen as the arm material as it has a low thermal conductance of 11 W/mK with a relatively high electrical conductance. The active VO_x film is encapsulated in silicon oxide to provide protection during necessary etching steps. An optically thick gold reflector sits on the substrate $2 \mu\text{m}$ below the VO_x film to facilitate a quarter-wave cavity for LWIR absorptance.

The read-out circuit is a voltage divider with an impedance-matched load resistor R_L . We measure the detector voltage V_{out} , which depends on R_L and applied bias V_B according to the voltage-divider formula [9], so that the change in voltage caused by IR-induced change in R is

$$dV_{\text{out}} = V_B \frac{R_L}{(R_L + R)^2} dR \approx \frac{V_B dR}{4R}, \quad (1)$$

where the last equality occurs because of the use of the matched load resistance. The voltage responsivity \mathcal{R}_v reported in this

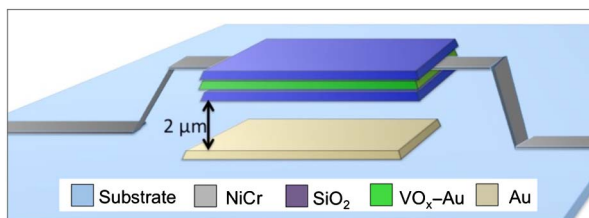


Fig. 1. Schematic diagram of the designed microbolometer used in testing.

paper is dV_{out} divided by the incident IR power, where V_B is the same for all measurements. The percent change in resistance dR/R is related to the change in device temperature by the temperature coefficient of resistivity (TCR) of the VO_x film, defined as

$$\text{TCR} \equiv \alpha = \frac{1}{R} \frac{dR}{dT}. \quad (2)$$

Voltage responsivity \mathcal{R}_v can also be expressed as [9]

$$\mathcal{R}_v = \frac{\mathcal{R}_0}{\sqrt{1 + (2\pi f)^2 \tau^2}}, \quad (3)$$

where

$$\mathcal{R}_0 = \frac{V_B \alpha \eta}{4G_{\text{eff}}} \quad (4)$$

is the responsivity when the modulation frequency $f = 0$. In Eq. (3), τ is the thermal time constant. In Eq. (4), η is the absorptance and G_{eff} the effective thermal conductance. According to Eq. (1), $4dV_{\text{out}}/V_B = \alpha dT$ so that \mathcal{R}_v is high when TCR and absorbed IR power are high and when heat capacity is low. Much research has raised the TCR of VO_x to the level of $\sim 2\%–3\%/K$ [2]. Thermal conductance in air-bridge bolometers can be decreased at the expense of a longer thermal time constant and decreased mechanical stability.

When a detector is irradiated by a blackbody source, the incident power on the detector is [9]

$$P_i(T) = L(T) \frac{A_{BB} A_d}{r^2} F_f t, \quad (5)$$

where A_{BB} is the blackbody area, A_d the detector area, r the distance from blackbody to detector, and t is the transmission of the window of the detector housing. The solid angle of the detector is approximated as A_{BB}/r^2 as $r \gg A_{BB}^{1/2}$. F_f is the form factor for the RMS value of the incident power to account for the modulation of the signal. Assuming square-wave modulation with 50% duty, $F_f = \sqrt{2}/\pi$ for the fundamental Fourier component. The radiance term L is determined by evaluating Planck's Law for the desired spectral range as

$$L = + \frac{2k^4 T^4}{h^3 c^2} \int_{x_2}^{x_1} \frac{x^3}{e^x - 1} dx, \quad x = \frac{hc}{\lambda k T}, \quad (6)$$

where T is the blackbody temperature, k_B is Boltzmann's constant, h is Planck's constant, and c is the speed of light in vacuum.

Responsivity can be improved by increasing the bias voltage at the expense of increased Johnson noise, which is given by [9]

$$V_j = \sqrt{4k_B T_d R \Delta f}, \quad (7)$$

where T_d is the device temperature, R is the resistance, and Δf is the measurement bandwidth, which is related to the measurement integration time τ_e by $\Delta f = 1/(2\tau_e)$ [9].

We previously estimated that our bolometers are Johnson noise limited [14], but results presented here show a $1/f$ characteristic to the noise at high bias voltages. The $1/f$ noise voltage is [17]

$$V_{1/f} = \sqrt{\frac{\left(\frac{V_B R}{R_L + R}\right)^M k_f}{f^N}}, \quad (8)$$

where $m \approx 2$, $n \approx 1$, and k_f is

$$k_f = \frac{\alpha_H}{nV}, \quad (9)$$

with α_H as the Hooge parameter, n is the mobile charge carrier density, and V is the volume of the material. Equation (7) presents the $1/f$ noise in units of V/\sqrt{Hz} . To compare with experiment, Eq. (8) must be integrated over the measurement bandwidth. Consensus is that $1/f$ noise arises from imperfections in the electrical paths and nonohmic contacts [18].

Adding an absorber increases the bolometer's heat capacity, which increases the thermal response time (and reduces device speed) according to [9]

$$\tau = \frac{C}{G} C = c_i \rho_i t_i A, \quad G = \frac{2g_{NiCr} t_{NiCr} w}{l}, \quad (10)$$

where C is the heat capacity determined by specific heat c_i , density ρ_i , thickness t_i , and area A of the SiO_2 and VO_x layers, and G is the thermal conductance through the two arms of the microbolometers, which is determined by arm geometry (t_{NiCr} , w , and l) and the thermal conductivity g_{NiCr} of NiCr.

3. EXPERIMENTAL DETAILS

Microbolometer design, fabrication, and testing procedures are described in [16]. A gold-doped VO_x thin film was formed as an air bridge with a 2 μm gap for Fabry–Perot resonant absorption, utilizing a 150 nm gold surface reflector. Revised numerical electrostatics calculations indicate an average absorptance of 71% for the LWIR. The gold in the VO_x reduces resistivity while maintaining high TCR [15]. 300 nm NiCr support arms in the air bridge minimizes thermal conduction while keeping the response time below 10 ms. The dimensions of the air bridge are 35 $\mu m \times 35 \mu m$, not including the arms.

Gold black was deposited and patterned by the lift-off technique described in [12,13]. Gold source material (99.999% purity) was thermally evaporated at 300 mTorr N_2 ambient. The low mean-free path inside the vacuum chamber causes gold atoms to collide and bind prior to landing on the thermoelectrically cooled substrate ($-13^\circ C$) [19]. The result is a pure gold in nanostructures of 5–30 nm in dimension, which can be modeled as an effective medium of gold and air. A photolithographic resist pattern of apertures was aligned to the bolometer array. For sufficient uniformity and thickness, multiple depositions were required with sample rotation between each deposition. The gold black was then encapsulated with 250 nm of e-beam evaporated SiO_2 prior to lift-off in acetone. One wafer containing hundreds of bolometers was fabricated and then cleaved in two to allow just half of the devices to receive a gold black coating. The uncoated bolometers served as references for comparison.

For characterization of absorptance, SiO_2 -coated gold black films were deposited onto gold-coated silicon substrates following procedures described in [12]. Specular and diffuse reflectance spectra were measured in a hemispherical directional reflectance spectrometer (SOC-100 HDR) connected to a

Fourier Transform Infrared Spectrometer (FTIR, Thermo Scientific) using unpolarized light at incident angles of 7° , 15° , 30° , 45° , and 60° . Transmittance was zero due to the gold film on the substrate, so that absorptance is unity minus the measured reflectance.

Absorptance of individual bolometers was measured using the imaging spectrometer at the University of Wisconsin, Milwaukee (formerly at the Synchrotron Radiation Center) [20]. A Bruker Vertex FTIR spectrometer equipped with a Hyperion 3000 infrared microscope was used to image the sample with a standard global source. A 128 \times 128 pixel focal plane array (FPA) detector was used to collect reflectance data over the 900–3700 cm^{-1} spectral range (2.7–11.1 μm) with a 4 cm^{-1} spectral resolution. A gold mirror was used for reference for the reflectance spectra. IRidys (infrared imaging and data analysis) software was used to analyze the spectrum collected by each pixel of the FPA. Absorptance was calculated as unity minus the reflectance, as the transmittance is zero due to the optically thick gold reflector under the pixel.

Infrared characterization of the effects of thermal processing on gold black was performed by collecting reflectance spectra at normal incidence from 3 to 15 μm wavelength. A Bomem DA8 Fourier spectrometer with a global source, KBr beam splitter, and 77 K HgCdTe detector were used. The substrates for the coatings used in these studies had a thick Au coating to ensure zero transmittance, so that absorptance is one minus reflectance. The reference spectrum for determining the reflectance was measured on a gold mirror.

The gold bond pads of the microbolometers were wire bonded to standard chip carriers using aluminum wire. These chip carriers were placed in a vacuum box with electrical feedthroughs. The window on the box was thallium bromide (KRS-5) with $\sim 70\%$ transmittance from 0.6 to 40 μm wavelength. The box was pumped below 20 mTorr to reduce thermal conduction and placed a distance $r = 14$ to 24 cm from a blackbody source (IR-301 Infrared Systems Development Corporation) with area $A_{BB} = 26.4 cm^2$. A blackbody temperature of $300^\circ C$ was used to achieve output voltages sufficiently above the noise floor without the use of a read-out amplifier. An optical chopper modulated the irradiance. The chopper surface facing the blackbody was highly reflective to avoid heating. The surface facing the detector was painted with high-temperature flat black paint to reduce reflections and to give high emissivity. Bolometer and load resistances were matched $R_L \approx R$, and the circuit was biased with a low-noise DC source. The modulation in V_{out} due to the chopped incident IR irradiance is the quantity dV_{out} [Eq. (1)], which was synchronously amplified using a lock-in (Stanford Research Systems 530) with a 30 ms time constant. The linear dependence of dV_{out} on V_B predicted by Eq. (1) was maintained up to 3 V. Thus, to stay within the range where Eq. (1) is valid, we kept V_B within the range of 1–3 V. The chopping frequency was set between 15 and 160 Hz, although most of the responsivity results reported here were measured at a chopping frequency of 80 Hz to reduce the $1/f$ noise contribution.

To characterize the noise [21], the incident blackbody irradiance was blocked by a shield whose highly reflecting surface

faced the blackbody, while carbon black was used on the surface facing the bolometer to obtain high emissivity. The noise is the output voltage variation measured using the lock-in amplifier with a time constant of 30 ms, so that the measurement bandwidth was 17 Hz.

The dependence of responsivity R_V on spectral bandwidth was determined using a variety of optical filters. For these measurements, detectors were biased at 3 V and chopped at 37 Hz. A germanium long-pass filter with 90% transmission from 7.6 to 14.6 μm was used to select the LWIR range. For MWIR characterization, a 3–5 μm optical filter with 90% transmission was used.

4. RESULTS

Figures 2(a) and 2(b) present SEM images of bolometers with and without gold black, respectively. The VO_x film is slightly inscribed within the pixel area, and it is protected on all sides by SiO_2 . The NiCr arms come into contact with the VO_x film on either side of the pixel, and they supported it above the substrate. The slight warping observed for the pixels affects mainly the Q of the Fabry–Perot resonant cavity formed by the air gap. The gold black film is uniform across the pixel, although it slopes down slightly around the edges. (The pixels shown in Fig. 2 have residual polyimide at the elbow joints of the arms. Such residues can also be seen with an optical microscope, which was used to confirm that such were absent from the pixels considered in responsivity studies).

Figure 3 presents the specular and diffuse reflectance spectra R for a gold black layer with 250 nm SiO_2 protection. No dependence on angle of incidence appears until angles of about 45°. Diffuse reflectance is <1% for the LWIR and is only ~1% for the MWIR, indicating negligible scattering. The spectrally averaged absorptance over the 8–12 μm LWIR wavelength band is ~70% for the smaller incidence angles, with a peak at 9.4 μm of 93% due to the SiO_2 . The absorptance averaged over the 3–5 μm MWIR wavelength band is ~86% for the smaller angles.

The lift-off process degrades the near-unity absorptance of pure gold black [12]. Even with the SiO_2 overcoat, absorptance has been shown to be near unity in both MWIR and LWIR,

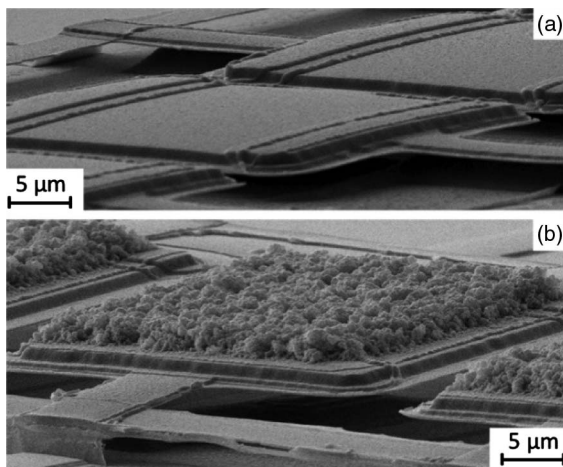


Fig. 2. VO_x air-bridge bolometers (a) without and (b) with the gold black coating.

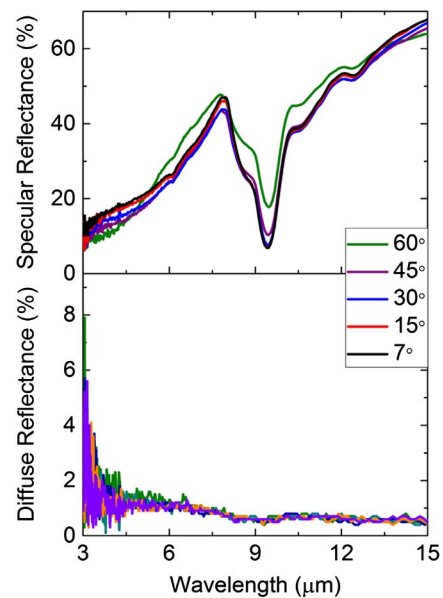


Fig. 3. Specular and diffuse reflectance of SiO_2 -protected gold black film on gold-coated silicon, at incidence angles of 7°, 15°, 30°, 45°, and 60°.

but the solvent bath used to facilitate patterning lift-off causes some collapse of the film, which results in a lower absorptance, particularly at longer wavelengths [12]. It is possible that a more complete encapsulation layer, either by a thicker or different material, could reduce this effect, but such investigations have yet to be done.

Figure 4 presents microscopic spatial maps of infrared spectral absorptance measured directly on fabricated devices and integrated over two standard wave bands, MWIR (3–5 μm) and LWIR (8–11 μm). Device absorptance includes the resonant absorption of Fabry–Perot cavity and of the SiO_2

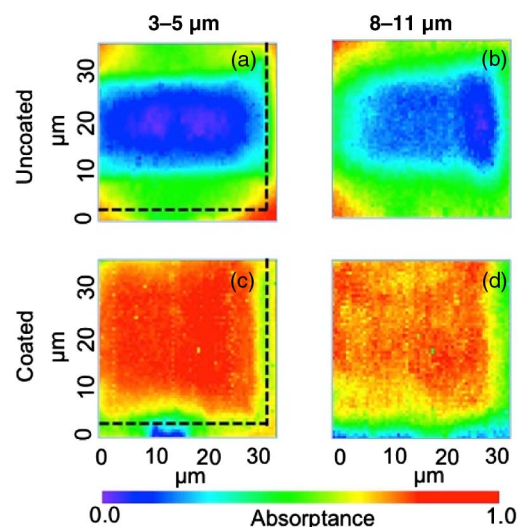


Fig. 4. Spatial absorptance map for an individual bolometer. (a),(b) The absorptance without gold black coating for MWIR and LWIR, respectively. The corresponding absorptance with the gold black coating is shown in images (c) and (d). The dashed line gives the outline of the air bridge.

in the air-bridge structure. All four images have the same $35\ \mu\text{m} \times 35\ \mu\text{m}$ field of view. The spatial sampling is $0.5\ \mu\text{m} \times 0.5\ \mu\text{m}$, so that the actual resolution is diffraction limited at all wavelengths. The pixel outline is represented by the black dashed line in images Figs. 4(a) and 4(c). The absorptance of bare pixels varies by 40% across the pixel, with the minimum at the center, where some points show almost zero absorption. The uncoated pixel's absorption is stronger in the LWIR than in the MWIR, due to the engineered Fabry–Perot resonance. However, the spatial uniformity is quite poor, which we attribute to the distortions in the FP cavity noted in Fig. 2. A gold black coating greatly increases the absorption and its uniformity across the pixel in both bands. There is a narrow region around the edges with weaker absorption, because the gold black is thinner there, as can be seen in Fig. 2.

Figure 5 presents absorptance spectra obtained from spatial-averages over the air-bridge area from the micro-FTIR imaging spectroscopy. For the uncoated sample, the Fabry–Perot absorption peak appears just beyond $8\ \mu\text{m}$ wavelength, and the SiO_2 absorption peak appears just beyond $9\ \mu\text{m}$. The latter is similar to the band observed for oxide-coated gold black (Fig. 3). When the coating is added, the absorption increases over the full $3\text{--}11\ \mu\text{m}$ wavelength range of the measurement. The maximum spatially averaged absorptance without gold black is only 48% for LWIR and 32% for MWIR. The presence of residual polyimide under the air bridge is likely the cause for these values to be significantly less than the 71% calculated peak LWIR absorptance. The gold black coating increases the average absorptance by 88% and 94% for the LWIR and MWIR, respectively. The absorptance spectrum of the coated bolometer is rather flat. The improvement is more in the MWIR than in the LWIR, where the bare device absorption was initially strongest and where the protected gold black absorption was weakest (Fig. 3).

For pure gold black, the index is ~ 1 , so that the Fresnel reflection at the gold-black–air interface is nearly zero [22,23]. Separate transmission and reflection measurements have also indicated that absorption is near unity for pure gold black [22,23]. However, as indicated in Figs. 3 and 5, the absorption of patterned, SiO_2 -coated gold black is somewhat less.

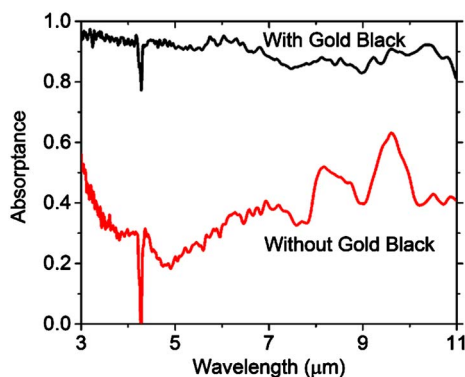


Fig. 5. Absorptance spectra averaged over one bolometer with and without gold black overcoat. The spike near $4.2\ \mu\text{m}$ is an artifact due to atmospheric CO_2 .

Indeed, the hint of the Fabry–Perot resonance at $8\ \mu\text{m}$ in the gold black spectrum indicates that some small fraction of light is indeed transmitting through the film. Absorptance for the coated device (Fig. 5) exceeds that for the coating alone (Fig. 3) because of contributions from the additional oxides and the cavity.

Fabrication yield was determined based on optical inspection and measured resistance. The most common failure is support-arm breakage, which results in an open circuit. Less common are electrical shorts from patterning misalignments. Inadequate or incomplete gold black coating occurs on fewer than 5% of pixels. Of the good pixels, we randomly selected and wire bonded 15 without the coating and 15 with the coating for testing. Detectors without gold black had an average resistance of $233 \pm 17.5\ \text{k}\Omega$, while coated detectors had an average resistance of $221 \pm 25\ \text{k}\Omega$. Load resistor values were selected in the range of $200\text{--}250\ \text{k}\Omega$ to match the device under test. The variation in the factor 4 in Eq. (1) due to imperfect load matching was less than 0.2%, so that the observed variations in dV_{out} reported below are due to other factors.

Figure 6 presents measured voltage responsivity values $\mathcal{R}_v = \frac{dV_{\text{out}}}{dP}$ as a function of detector resistance. Chopping frequency was 80 Hz and detector bias was 1 V. No optical filter was used, so the incident spectral range was defined by window transmittance to be $0.6\text{--}40\ \mu\text{m}$ wavelength. The peak of the 300°C blackbody temperature was in the MWIR. The average responsivity for detectors without gold black was $753 \pm 67\ \text{V/W}$, while the average responsivity for gold-black-coated samples was $1110 \pm 126\ \text{V/W}$. Thus, the coating improved the responsivity by 47%, which is much more than the 9% and 11% statistical uncertainties for the \mathcal{R}_v values

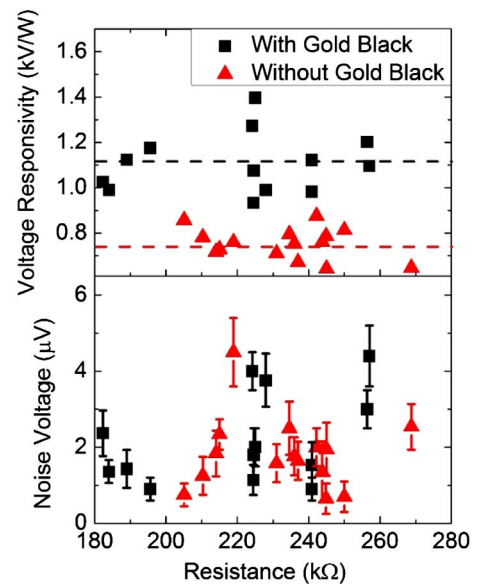


Fig. 6. Measured voltage responsivity and noise voltage over a range of detectors, displayed as a function of detector resistance. Measurements are made at 80 Hz chopping frequency with 1 V applied bias and no optical filter. A 300°C blackbody temperature was used. The noise measurements had a degree of uncertainty, which is indicated by error bars. Uncertainty in responsivity was less than the symbol size.

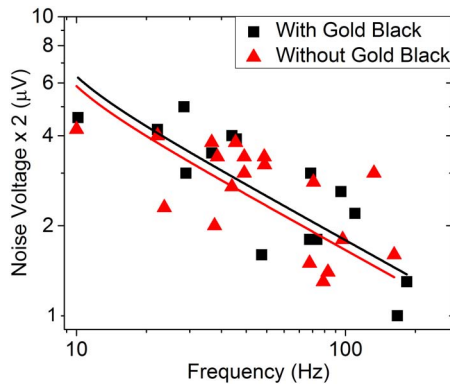


Fig. 7. Measured noise voltage (symbols) as a function of frequency for five devices with gold black compared with five uncoated device, plotted as twice the noise voltage to show a full decade in the vertical scale. The slope of the line in this scale is approximately -0.5 .

within each group, respectively. TCR goes as $\log(R)$ [9], so that the variation in \mathcal{R}_v should be small over the range of resistances plotted in Fig. 6. In fact, no trend in \mathcal{R}_v is observed comparable to the statistical variations. This justifies the averaging represented by the horizontal dashed lines in Fig. 6.

The measured noise is presented in the lower part of Fig. 6. The values exceed the ~ 250 nV expected for Johnson noise by a factor 10. While thermal fluctuation noise and photon noise contribute very little to the total device noise, the magnitude of $1/f$ noise is less easy to predict. To investigate the frequency dependence of the noise, five samples with gold black and five without gold black were chosen at random from samples with resistances in the range of Fig. 6. Figure 7 presents a plot of the frequency dependence of the measured noise voltage. Here, the noise voltage is doubled to show a full decade in the vertical scale. Fits of Eq. (8) (integrated over the 17 Hz measurement bandwidth) with $\kappa = \frac{\alpha_H}{nV}$ as the fitting parameter are plotted in Fig. 7 and confirm the $1/f$ nature of the noise. The slope of the fitted lines is approximately -0.5 on the log scale, indicating the dependence on V of $f^{-1/2}$, as indicated in Eq. (8). The difference between the two curves is clearly much less than the statistical variation of the data, so that we conclude that gold black causes no increase in the noise. Using the volume of the VO_x film, we find values for the normalized Hooge parameter $\frac{\alpha_H}{n} \sim 1.5 \times 10^{-22} \text{ cm}^3$. Wood [18] reports a similar value of $\frac{\alpha_H}{n} \sim 10^{-22} \text{ cm}^3$ for VO_x films developed at Honeywell, while Basantani *et al.* [24] reports values in the range of 10^{-17} – 10^{-22} cm^3 , with larger values holding for high resistivity VO_x films.

Figure 8 presents \mathcal{R}_v for one pixel as a function of chopping frequency from 10 to 150 Hz for detectors with and without gold black. The applied bias was 1 V, and no optical filter was used in this data. Values are excluded near 60 Hz due to high noise. By fitting these data with the function in Eq. (3), the parameters for \mathcal{R}_0 and τ_{th} were determined. This fit (solid lines) shows that the DC responsivity increases from 4.13 to 6.24 kV/W by adding gold black, an increase of 51%, while the thermal response time only increases by 15%, from 9.57 to 10.97 ms. Hence, a marginal decrease in device speed is observed.

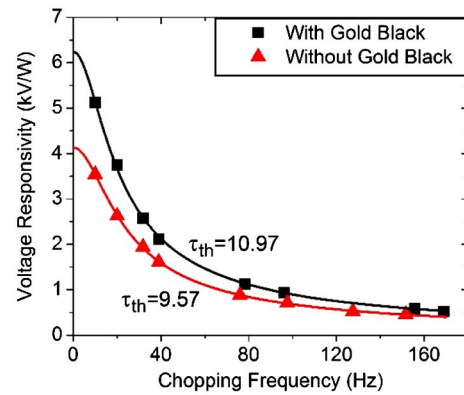


Fig. 8. Measured voltage responsivity as a function of chopping frequency. The solid lines are fits to Eq. (1). 1 V bias, 300°C blackbody temperature.

The values determined from the fitting parameter \mathcal{R}_0 allow an estimate of the thermal conductance G from Eq. (4). The TCR is assumed to be $-2.0\%/K$ based upon measurements of witness samples, and the absorptance for bare and coated samples is taken as the average over the 3–11 μm wavelength range from Fig. 5, namely, 0.54 and 0.85, respectively. We obtain thermal conductance G values of $6.5 \times 10^{-7} \text{ W K}^{-1}$ and $6.8 \times 10^{-7} \text{ W K}^{-1}$, respectively, i.e., an increase of 4% caused by the coating. The smallness of this increase emphasizes that the main thermal conductance path is the arms, which are unaffected by the coating.

The fitting parameter τ and the just-determined value for G allow an estimate of heat capacity C using Eq. (10). For bare and coated bolometers we find $C = 6.26 \times 10^{-9}$ and $7.47 \times 10^{-9} \text{ J K}^{-1}$, respectively, i.e., the coating increases C by 19%. The density of protected gold black after lift-off was estimated to be 8% of bulk gold [16], so a 2 μm thick layer of gold black with 250 nm SiO_2 should add $0.87 \times 10^{-9} \text{ J K}^{-1}$ to the heat capacity, or a 14% increase, which is in reasonable agreement with the value obtained from the fit. Thus, the speed limitation of a device by the increase in heat capacity is small.

Figure 9 presents the effect of restricting the spectral range with an optical filter on the responsivity improvement achieved with gold black coating. Without an optical filter, the bandwidth incident on the detector was window limited to the range of 0.6–40 μm wavelength, but there is effectively no irradiance beyond about 15 μm , according to the 300°C blackbody curve also plotted in Fig. 9. The responsivity improvement is smallest for the LWIR band, where the uncoated bolometers already had significant absorption due to the FP cavity and the oxide. The improvement for the MWIR band is much larger and is comparable to that obtained over the full unfiltered band. Responsivity improvements follow the absorptance improvements for the same bands.

Gold black is vulnerable to thermal processing [22,23]. Commercial IR cameras require the detector array to be vacuum-sealed. Usual vacuum sealing processes heat the array above 300°C [25,26], which is expected to degrade the absorption of gold black significantly. To verify, a sample coated in

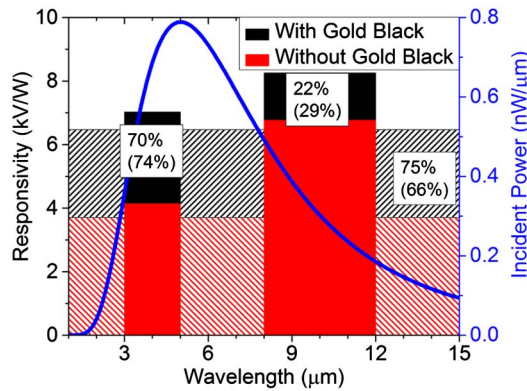


Fig. 9. Measured voltage responsivity as a function of IR bandwidth, which is given by horizontal limits of each bar. The solid curve is the calculated incident power spectrum based on the blackbody radiance at 300°C. Upper percentage labels give the responsivity increase due to the gold black coating, while the lower values in parentheses give the absorptance increase for the same range. (The range for LWIR responsivity is somewhat larger than for absorptance, which terminates at 11 μm wavelength.) 3 V bias, 300°C blackbody, 37 Hz chopping frequency.

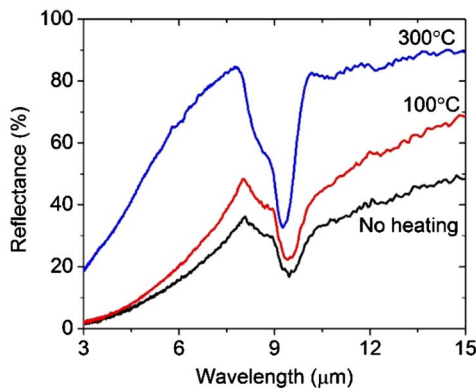


Fig. 10. Reflectance spectra of gold black after annealing at the indicated temperatures for 10 min.

gold black with the evaporated SiO₂ overcoat protection layer was broken into three pieces. One was kept as the reference. The other two were heated on a hot plate for 10 min at 100°C and 300°C, respectively. Figure 10 presents the reflectance spectra, which show that the heat treatment increases the reflectance and hence degrades the absorption. The sample heated to 300°C turned from black to dark red, and SEM imaging shows that this gold black has collapsed and begun to coalesce. The thermal degradation of gold black indicates the need for new low-temperature methods of vacuum packaging for arrays so coated. Research in low-temperature vacuum sealing is ongoing [27,28].

5. DISCUSSION AND SUMMARY

The integration of patterned gold black with a microbolometer has been presented. Experimental analysis demonstrates the

potential for a dual band, wide-angle absorber for improving the responsivity of room-temperature bolometer arrays. The gold black creation, application, protection, and patterning processes must be integrated into the device fabrication flow. Such coatings cannot be applied after releasing the fragile air-bridge structures.

Responsivity improvements as high as ~75% were observed for our devices averaged over both bands using the 300°C blackbody as a test object. Most of the applications for LWIR bolometers are for scenes closer to room temperature. To estimate how our results would differ if we had used a room-temperature blackbody, we note that responsivity is proportional to the weighted spectral average of the device absorptance, where the weighting function is the Planck function. Using the bare-bolometer absorptance spectrum from Fig. 5, we find that the difference in uncoated-bolometer responsivity between room temperature and 300°C blackbody scenes is only about 10% in any of the bands considered. The absorptance of the coated device has a flat spectrum (Fig. 5), so that the effect of scene temperature on responsivity of coated bolometers is very small. Thus, the improvements due to the coating depend only weakly on scene temperature.

Responsivity and Noise Equivalent Power of our devices may fall short of what is already commercially available, but absorptance is a key enabler for high responsivity, and the approach we report achieves absorptance that is competitive with the state of the art [8]. Thus, our approach may suggest an alternative approach to fabrication of high-performance LWIR room-temperature bolometers with possible manufacturing advantages such as relaxed tolerances and lower cost.

Our coating increased the thermal time constant of our bolometers by ~15%, but they remain sufficiently fast for standard 30 Hz video frame rates. A vacuum packaging method that maintains array temperatures below 100°C would be required to avoid degrading the gold black coatings. High responsivity in both MWIR and LWIR simultaneously may suggest new applications, such as multispectral imaging and the possibility of increasing dynamic range for scenes that contain both hot and room-temperature objects.

Funding. U.S. Army Research Labs Small Business Innovation Research (SBIR) (W911QX-13-C-0013); National Science Foundation (NSF) (CHE-1508240, CHE-1112433).

Acknowledgment. We acknowledge the support and assistance from Mr. Guy Zummo, Mr. Ed Dein, and Prof. Kevin Coffey. Also we extend thanks to Alvar Rodriguez for wire bonding assistance and to Farnood Khalilzadeh-Rezaie for help with the curve fitting.

REFERENCES

1. S. R. Hunter, R. A. Amantea, L. A. Goodman, D. B. Kharas, S. Gershtein, J. R. Matey, S. N. Perna, Y. Yu, N. Maley, and L. K. White, "High sensitivity uncooled microcantilever infrared imaging arrays," *Proc. SPIE* **5074**, 469–480 (2003).
2. F. Niklaus, C. Vieider, and H. Jakobsen, "MEMS-based uncooled infrared bolometer arrays—a review," *Proc. SPIE* **6836**, 68360D (2007).
3. N. Liu, M. Mesch, T. Weiss, M. Hentschel, and H. Giessen, "Infrared perfect absorber and its application as plasmonic sensor," *Nano Lett.* **10**, 2342–2348 (2010).

4. C. M. Watts, X. Liu, and W. J. Padilla, "Metamaterial electromagnetic wave absorbers," *Adv. Mater.* **24**, 98–120 (2012).
5. S. Ogawa, J. Komoda, K. Masuda, and M. Kimata, "Wavelength selective wideband uncooled infrared sensor using a two-dimensional plasmonic absorber," *Proc. SPIE* **8704**, 8704181 (2013).
6. Q. Cheng, S. Paradis, T. Bui, and M. Almasri, "Design of dual-band uncooled infrared microbolometer," *Sens. J.* **11**, 167–175 (2011).
7. M. Aggoun, J. Jiang, and M. K. Khan, "Infrared absorption modeling of VO_x microbolometer," *Proc. SPIE* **9620**, 962000 (2015).
8. D. Murphy, M. Ray, J. Wyles, C. Hewitt, R. Wyles, E. Gordon, K. Almada, T. Sessler, S. Baur, D. Van Lue, and S. Black, "640 × 512 17 μm microbolometer FPA and sensor development," *Proc. SPIE* **6542**, 65421Z (2007).
9. E. L. Dereniak and G. D. Boreman, *Infrared Detectors and Systems* (Wiley, 1996).
10. J. Murguia, Solid State Scientific Corp., Nashua, NH 03060 (private communication, 2015).
11. W. Becker, R. Fettig, A. Gaymann, and W. Ruppel, "Black gold deposits as absorbers for far infrared radiation," *Phys. Stat. Sol. (B)* **194**, 241–255 (1996).
12. D. Panjwani, M. Yesiltas, J. Nath, D. E. Maukonen, I. Rezaad, E. M. Smith, R. E. Peale, C. Hirschmugl, J. Sedlmair, R. Wehlitz, and M. Unger, "Patterning of oxide-hardened gold black by photolithography and metal lift-off," *Infrared Phys. Technol.* **62**, 94–99 (2014).
13. D. Panjwani, "Infrared detector with metal-black coating having dielectric overlayer and related methods," U.S. patent 20,140,374,597 (25 December 2014).
14. E. M. Smith, J. C. Ginn, A. P. Warren, C. J. Long, D. Panjwani, R. E. Peale, and D. J. Shelton, "Linear bolometer array using a high TCR VO_x-Au film," *Proc. SPIE* **9070**, 90701Z (2014).
15. K. R. Coffey, V. H. Lam, E. Dein, A. P. Warren, G. Boreman, G. V. Zummo, and W. Caba, "Nanocomposite semiconducting material with reduced resistivity," U.S. patent 8,228,159 (24 July 2012).
16. E. M. Smith, D. Panjwani, J. C. Ginn, A. P. Warren, C. J. Long, P. Figueredo, C. Smith, J. Perlstein, N. Walter, C. Hirschmugl, and R. E. Peale, "Enhanced performance of VO_x-based bolometer using patterned gold black absorber," *Proc. SPIE* **9451**, 94511I (2015).
17. P. W. Kruse, *Uncooled Thermal Imaging: Arrays, Systems, and Applications* (SPIE, 2001).
18. R. Wood, *Monolithic Silicon Microbolometer Arrays*, P. W. Kruse and D. D. Skatrud, eds., in *Uncooled Infrared Imaging Arrays and Systems* (Academic, 1997), pp. 43–121.
19. D. Panjwani, "Metal Blacks as Scattering Centers to Increase Efficiency of Thin Film Solar Cells," Master's thesis (University of Central Florida, 2011).
20. M. J. Nasse, M. J. Walsh, E. C. Mattson, R. Reininger, A. Kajdacsy-Balla, V. Macias, R. Bhargava, and C. J. Hirschmugl, "High resolution Fourier-transform infrared chemical imaging with multiple synchrotron beams," *Nat. Methods* **8**, 413–416 (2011).
21. ASTM Standard E1543-00 (2012), "Standard test method for noise equivalent temperature difference of thermal imaging systems," ASTM International, West Conshohocken, PA (2012), www.astm.org.
22. D. Panjwani, *Characterization of Gold Black and its Applications in Uncooled Infrared Detectors* (University of Central Florida, 2015).
23. D. Panjwani, A. Dutta, J. Nath, H. Heinrich, and R. E. Peale, "Aging of nano-morphology, resistivity, and far-infrared absorption in gold-black," *J. Appl. Phys.* **118**, 154307 (2015).
24. H. A. Basantani, D. B. Saint John, N. J. Podraza, T. N. Jackson, and M. W. Horn, "Evaluation of 1/f noise in prospective IR imaging thin films," *Proc. SPIE* **9070**, 90701P (2014).
25. F. Forsberg, N. Roxhed, A. C. Fischer, B. Samel, P. Ericsson, N. Hoivik, A. Lapadatu, M. Bring, G. Kittilsland, G. Stemme, and F. Niklaus, "Very large scale heterogeneous integration (VLSHI) and wafer-level vacuum packaging for infrared bolometer focal plane arrays," *Infrared Phys. Technol.* **60**, 251–259 (2013).
26. R. E. Higashi, J. A. Ridley, T. G. Stratton, and R. A. Wood, "Integrated silicon vacuum micropackage for infrared devices," U.S. patent 5,895,233 (20 April 1999).
27. S. P. Stagon and H. Hanchen, "Airtight metallic sealing at room temperature under small mechanical pressure," *Sci. Rep.* **3**, 3066 (2013).
28. S. Garcia-Blanco, P. Topart, Y. Desroches, J. S. Caron, F. Williamson, C. Alain, and H. Jerominek, "Low-temperature vacuum hermetic wafer-level package for uncooled microbolometer FPAs," *Proc. SPIE* **6884**, 68840P (2008).